Multiple classical noise mitigation by multiobjective robust quantum optimal control

Bowen Shao,[1] Xiaodong Yang ©,[2,*] Ran Liu,[2] Yue Zhai,[1] Dawei Lu,[1,3] Tao Xin,[1,3,†] and Jun Li[2,‡]

[1]*Shenzhen Institute for Quantum Science and Engineering, Southern University of Science and Technology, Shenzhen 518055, China*

[2]*College of Physics and Optoelectronic Engineering, Shenzhen University, Shenzhen 518060, China*

[3]*Guangdong Provincial Key Laboratory of Quantum Science and Engineering, Southern University of Science and Technology, Shenzhen 518055, China*

High-quality control is a fundamental requirement for quantum computation, but practically it is often hampered by the presence of various types of noises, which can be static or time dependent. In many realistic scenarios, multiple noise sources coexist, and their resulting noise effects need to be corrected to a sufficient order, posing significant challenges for the design of effective robust control methods. Here, we explore the method of robust quantum optimal control to generally tackle the problem of resisting multiple noises from a complicated noise environment. Specifically, we confine our analysis to classical stochastic noises that can be described by classical noise models. This method employs a gradient-based multiobjective optimization algorithm to maximize the control figure of merit, and meanwhile to minimize the perturbative effects of the noises that are allowed for. To verify its effectiveness, we apply this method to a number of examples, including robust entangling gate in a trapped-ion system and robust controlled-*Z* gate in superconducting qubits, under commonly encountered static and time-dependent noises. Our simulation results reveal that robust optimal control can find smooth, robust pulses that can simultaneously resist several noises and thus achieve high-fidelity gates. Therefore, we expect that this method will find wide applications on current noisy quantum computing devices.

I. INTRODUCTION

For reliable quantum computation, it is a vital task, but a challenging one, to precisely manipulate quantum systems in the presence of various noises [1]. In reality, noises may originate from a variety of sources, including inaccurate dynamical modeling, unstable system parameters, imperfect controls, inevitable interactions with environment, imprecise measurements, etc. [2,3]. Quantum error correction can generally suppress the noises to a desired level [4]. However, in the noisy intermediate-scale quantum (NISQ) era [5], it is still prohibitive to realize quantum error correction, as encoding a single logical qubit needs thousands of physical qubits and extensive quantum operations below certain precision thresholds [6,7]. Therefore, significant efforts should be made on developing practical strategies, for example, error mitigation [8], and robust quantum control [9], to tackle the noise issue.

Substantial tremendous robust quantum control methods have been proposed in recent decades, such as composite

─────────
*yangxd@sustech.edu.cn
†xint@sustech.edu.cn
‡lij3@sustech.edu.cn

pulses [10–12], dynamical decoupling [13–15], geometric-formalism-based pulse control [16,17], and sampling-based learning control [18,19]. Although these robust control methods have been used in various experiments, their application to general quantum engineering tasks still face a number of challenges: (i) Many of the mentioned methods consider the noise effects perturbatively in an analytical manner, and thus usually restricted to only the low-order perturbative expansion terms. However, in situations where achieving high-precision target operations is necessary, it is desirable to take the higher-order noise effects into account [16,20]. (ii) Existing methods usually behave well when the noises are quasistatic, but this assumption is not always valid [21]. There have been a lot of noise spectroscopy experiments in recent years, revealing that time-dependent noises are commonly found in many quantum platforms [22–25]. How to resist realistic time-dependent noises with robust control currently remains a difficult task. (iii) Previously, robust control usually considers resisting one to two types of noises. However, as indicated by recent randomized benchmarking experiments, there often exist multiple noises in real quantum devices, which must be simultaneously considered for further improvement of control fidelities

[26,27]. (iv) Realistic noises may have temporal or spatial correlations [28], which poses an extra challenge for current robust control methods. Furthermore, things get more complicated when the system size becomes large. Therefore, a practical robust control method, which can handle the aforementioned issues towards NISQ applications, is still under urgent demand.

In this work, we study a general robust quantum optimal control method to fight against multiple sources of noises simultaneously. Quantum optimal control functions by minimizing a settled cost function subject to adjustable control parameters with an appropriate optimization algorithm [2]. To allow for the noise impacts, following Ref. [29], we adopt the concept of directional derivative, which quantifies the variation of the time-evolution operator caused by given noises. The different orders of directional derivatives can be evaluated via the Van Loan integral formula [30], and we use their norms as additional cost functions for consideration of robustness. We shall employ the widely used gradient-ascent pulse engineering (GRAPE) [31] technique for pulse optimization, hence we refer to the whole algorithm as Van Loan GRAPE. Moreover, we add practical constraints of bounded and smoothly varying control amplitudes in optimization. Therefore, our method is essentially to solve a multiobjective optimization problem. As demonstration examples, we apply the method to search robust optimal control (ROC) pulses for realizing the Mølmer-Sørensen (MS) gate in a trapped-ion system and the controlled-Z gate in a superconducting system. Various types of noise are considered in these test examples, including both static noises and time-dependent noises. The simulation results reveal that our method is capable of designing robust pulses under complex noisy circumstances for high-quality controls. The outline of this work is given as follows. We first introduce Van Loan GRAPE in detail in Sec. II. Applications in trapped ions and superconducting qubits are then demonstrated in Sec. III and Sec. IV, respectively. Finally, we give brief conclusions and discussions in Sec. V.

II. METHOD

Consider a controlled quantum system governed by the Schrödinger equation

$$\dot{U}(t) = -i[H_S + H_C(u(t))]U(t), \tag{1}$$

with $U(0) = \mathbb{1}$ (identity matrix), where H_S is the system Hamiltonian, $H_C(t)$ represents the control Hamiltonian, and $u(t)$ denotes the time-dependent controls. The solution of the above equation at time $t = T$ can be formally written as

$$U(T) = \mathcal{T} \exp\left(-i \int_0^T dt[H_S + H_C(u(t))]\right),$$

where $\mathcal{T}$ is the time-ordering operator. An essential objective in quantum control is the realization of a desired quantum gate denoted as U_{tar}. This task is typically accomplished by quantum optimal control techniques [2], which involve the maximization of the following gate fidelity function with adjustable controls, i.e.,

$$\Phi_0(u) = |\operatorname{Tr}(U(T) \cdot U_{\text{tar}}^\dagger)|^2/d^2, \tag{2}$$

where d represents the system dimension.

A. Noise perturbation

We now consider that there exist multiple noises during control, which result in deviations of the actual system evolution from the ideal noise-free evolution. The total evolution operator $U_{\text{tot}}(t)$ with noises can be described by

$$\dot{U}_{\text{tot}}(t) = -i[H_S + H_C(t) + H_V(t)]U_{\text{tot}}(t), \tag{3}$$

where $H_V(t) = \sum_j \epsilon_j(t)E_j(t)$ is the perturbed Hamiltonian, $\epsilon_j(t)$ represents the jth noise, and E_j denotes the corresponding noise operator. The solution of Eq. (3) can be formally expressed as

$$U_{\text{tot}}(t) = \mathcal{T} \exp\left(-i \int_0^t dt_1[H_S + H_C(t_1) + H_V(t_1)]\right),$$

which is, however, often difficult to calculate because the noise $\epsilon_j(t)$ may vary with time randomly. For each time instance, the overall evolution is a unitary process, allowing us to take the ensemble average of the noises to define the gate-fidelity function corresponding to Eq. (2), i.e.,

$$\Phi_{\text{noise}}(u) = \langle |\operatorname{Tr}[U_{\text{tot}}(T)U_{\text{tar}}^\dagger]|^2/d^2 \rangle, \tag{4}$$

where $\langle \cdot \rangle$ represents the ensemble average. If the noise evolves slowly relative to the timescales of the controls, it can be considered quasistatic, i.e., $\epsilon_j(t) = \epsilon_j$, thus in this case the gate fidelity can be simplified to

$$\Phi_{\text{noise}}(u) = |\operatorname{Tr}[U_{\text{tot}}(T)U_{\text{tar}}^\dagger]|^2/d^2. \tag{5}$$

To analyze the noise effects, we move to the toggling frame, where the evolution propagator is defined as

$$\tilde{U}(t) = \mathcal{T} \exp\left(-i \int_0^t dt_1 \tilde{H}_V(t_1)\right), \tag{6}$$

with $\tilde{H}_V(t) = U^\dagger(t)H_V(t)U(t)$. With these definitions, it holds that $U_{\text{tot}}(t) = U(t)\tilde{U}(t)$, which conveniently separates the effects of noise from the overall evolution. Subsequently, we expand $\tilde{U}(t)$ with Dyson series [32] under the

condition that $\epsilon_j(t)$ is small enough, thus get

$$
U_{\text{tot}}(t) = U(t) \left[\mathbb{1} - i \sum_j \int_0^t dt_1 \epsilon_j(t_1) \tilde{E}_j(t_1) + (-i)^2 \right.
$$

$$
\left. \times \sum_{j,k} \int_0^t dt_1 \int_0^{t_1} dt_2 \epsilon_j(t_1) \epsilon_k(t_2) \tilde{E}_j(t_1) \tilde{E}_k(t_2) + \cdots \right].
\tag{7}
$$

Generally speaking, the noise effects can be mitigated by reducing the above perturbation terms order by order. There exist several studies that attempt to analytically find robust controls for minimizing the perturbation terms [16,17]. However, these methods can consider only the lower orders of the perturbation and one to two types of noises due to the complexity of analysis. To practically quantify and minimize the noise effects, we take use of directional derivatives as proposed in Ref. [29] in the optimization process. As the calculations of directional derivatives differ slightly depending on whether or not the noise is time dependent, we clarify in two different scenarios as follows.

B. Directional derivatives for time-independent noise

If the noise ϵ_j is constant, i.e., the noise value does not change with time, then it can be directly separated from the integral expressions in Eq. (7). The directional derivatives are defined as different orders of derivatives of $U_{\text{tot}}(t)$ with respect to ϵ_j at $\epsilon_j = 0$ [29]. For example, the first-order

directional derivative is

$$
\mathcal{D}_U^{(1)}(E_j) \equiv \left. \frac{dU_{\text{tot}}(t)}{d\epsilon_j} \right|_{\epsilon_j = 0} = -iU(t) \int_0^t dt_1 \tilde{E}_j(t_1),
\tag{8}
$$

and the second-order directional derivative reads

$$
\mathcal{D}_U^{(2)}(E_j, E_k) \equiv \left. \frac{d^2 U_{\text{tot}}(t)}{d\epsilon_j \, d\epsilon_k} \right|_{\epsilon_j, \epsilon_k = 0}
$$

$$
= -2U(t) \int_0^t dt_1 \int_0^{t_1} dt_2 \tilde{E}_j(t_1) \tilde{E}_k(t_2).
$$

The other orders of directional derivatives can be similarly derived. By utilizing directional derivatives, we can measure the extent to which a system's evolution deviates from its ideal evolution trajectory due to the presence of noise. However, calculating these derivatives is not an easy task, as it involves resource-consuming integral procedures.

To make the computation of the directional derivatives easier, we apply the technique of the Van Loan integral formula [29,30]. We begin by introducing a block matrix $B(t)$ that incorporates N types of noises defined by the corresponding noise operators $E_j(t), j = 1, 2, \ldots, N$, i.e.,

$$
B(t) = \begin{pmatrix} H(t) & E_1(t) & 0 & \ldots & 0 \\ 0 & H(t) & E_2(t) & \ldots & 0 \\ \vdots & \vdots & \vdots & \ddots & \vdots \\ 0 & 0 & 0 & \ldots & E_N(t) \\ 0 & 0 & 0 & \ldots & H(t) \end{pmatrix},
\tag{9}
$$

where $H(t) = H_S + H_C(t)$. Moreover, we assume that it obeys the differential equation $\dot{V}(t) = -iB(t)V(t)$ with $V(0)$ being the identity matrix. According to the Van Loan integral formula [30], the solution of this equation at $t = T$ can then be calculated as

$$
V(T) = \mathcal{T} \exp\left(-i \int_0^T B(t)dt \right) = \begin{pmatrix} U(T) & \mathcal{D}_U^{(1)}(E_1)(T) & \mathcal{D}_U^{(2)}(E_1, E_2)(T) & \ldots & \mathcal{D}_U^{(N)}(E_1, \ldots, E_N)(T) \\ 0 & U(T) & \mathcal{D}_U^{(1)}(E_2)(T) & \ldots & \mathcal{D}_U^{(N-1)}(E_2, \ldots, E_N)(T) \\ \vdots & \vdots & \vdots & \ddots & \vdots \\ 0 & 0 & 0 & \ldots & \mathcal{D}_U^{(1)}(E_N)(T) \\ 0 & 0 & 0 & \ldots & U(T) \end{pmatrix}.
\tag{10}
$$

Therefore, by expressing the noise-free Hamiltonian $H(t)$ and the noise operators $E_j(t)$ as a block matrix $B(t)$ in the form shown in Eq. (9), we can easily obtain the directional derivatives from the off-diagonal terms of the time-evolution operator $V(T)$ in Eq. (10).

C. Directional derivatives for time-dependent noise

For time-dependent noise, we routinely assume that each $\epsilon_j(t)$ is a stationary Gaussian process with zero

mean, i.e., $\langle \epsilon_j(t) \rangle = 0$. Additionally, we assume that each pair of the noises is mutually independent, namely $\langle \epsilon_j(t_1)\epsilon_k(t_2) \rangle = 0$ when $j \neq k$. Under these assumptions, we can characterize each time-dependent noise with its correlation functions [33,34]. For simplicity, we consider only the autocorrelation function $\langle \epsilon_j(t_1)\epsilon_j(t_2) \rangle$ and denote $\langle \epsilon_j(t_1)\epsilon_j(t_2) \rangle \equiv \epsilon_j^2 \langle \tilde{\epsilon}_j(t_1)\tilde{\epsilon}_j(t_2) \rangle$, where ϵ_j represents the noise strength for the jth noise and $\tilde{\epsilon}_j(t)$ is the corresponding normalized time-dependent noise.

Usually, the noise has a decaying autocorrelation function, and in such cases, we can approximate the autocorrelation function using a linear combination of exponential functions, i.e., $\langle \tilde{\epsilon}_j(t_1)\tilde{\epsilon}_j(t_2) \rangle = \sum_i a_{ji} e^{b_{ji}(t_2-t_1)}, 0 < t_1 < t_2 < T$. For example, the autocorrelation function of the typical dephasing noise in nitrogen-vacancy center system is proportional to an exponential function $e^{-\gamma|t|}$ [35]. With neglecting cross-correlations between the noises, and taking the noise ensemble average of Eq. (7), the equation can be simplified as $\langle U_{\text{tot}} \rangle = U(t)\left[\mathbb{1} - \sum_j \int_0^t dt_1 \int_0^{t_1} dt_2 \langle \epsilon_j(t_1)\epsilon_j(t_2)\rangle \tilde{E}_j(t_1)\tilde{E}_j(t_2)\right] = U(t)\left[\mathbb{1} - \sum_{j,i} \epsilon_j^2 \int_0^t dt_1 \int_0^{t_1} dt_2 a_{ji} e^{b_{ji}(t_2-t_1)} \tilde{E}_j(t_1)\tilde{E}_j(t_2)\right]$. Similarly, the second-order directional derivative can be expressed by

$$
\begin{aligned}
&\mathcal{D}_U^{(2)}(\epsilon_j(t)E_j, \epsilon_j(t)E_j) \\
&= -2\sum_i U(t) \int_0^t dt_1 \int_0^{t_1} dt_2 a_{ji} e^{b_{ji}(t_2-t_1)} \tilde{E}_j(t_1)\tilde{E}_j(t_2) \\
&= \sum_i a_{ji}\mathcal{D}_U^{(2)}(e^{b_{ji}}E_j, e^{-b_{ji}}E_j). \qquad (11)
\end{aligned}
$$

Now, to calculate the above directional derivative, we again use the the technique of the Van Loan integral formula [29,30]. Concretely, we introduce a set of block matrices for each time-dependent noise $\epsilon_j(t)$

$$
C_{ji}(t) = \begin{pmatrix} H(t) & e^{b_{ji}t}E_j(t) & 0 \\ 0 & H(t) & e^{-b_{ji}t}E_j(t) \\ 0 & 0 & H(t) \end{pmatrix}, \qquad (12)
$$

and solve the corresponding differential equation $\dot{V}_{ji}(t) = -iC_{ji}(t)V_{ji}(t)$. According to the Van Loan integral formula, the solution of this equation at $t = T$ is

$$
V_{ji}(T) = \begin{pmatrix} U(T) & * & \mathcal{D}_U^{(2)}(e^{b_{ji}}E_j, e^{-b_{ji}}E_j)(T) \\ 0 & U(T) & * \\ 0 & 0 & U(T) \end{pmatrix},
$$

where the element signified by $*$ is not relevant to our calculations and thus is not shown explicitly. Therefore, the directional derivative in Eq. (11) can be conveniently calculated using the off-diagonal term in the above equation.

D. Fitness function and optimization procedure

From the above descriptions, we clearly see that the directional derivatives can quantitatively characterize the noise perturbative effects of different orders. To find robust controls that can achieve the control target and meanwhile mitigate the noise effects, we introduce the following
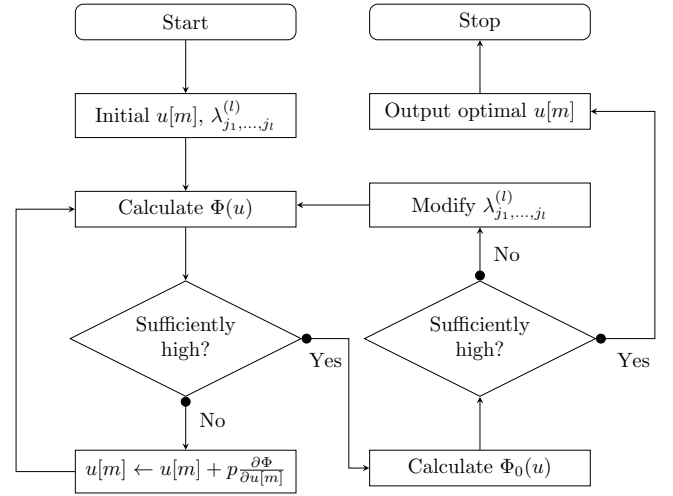

FIG. 1. Flowchart of the Van Loan GRAPE algorithm. The algorithm starts by guessing a random initial control pulse. After a number of iterations, the algorithm produces a high-fidelity robust optimal control pulse.

multiobjective fitness function:

$$
\Phi(u) = \Phi_0(u) - \sum_l \sum_{j_1,\dots j_l} \lambda_{j_1,\dots,j_l}^{(l)} \left\| \mathcal{D}_U^{(l)}\left(E_{j_1},\dots,E_{j_l}\right) \right\|^2, \qquad (13)
$$

where $\Phi_0(u)$ is the gate-fidelity function introduced above, $\mathcal{D}_U^{(l)}\left(E_{j_1},\dots,E_{j_l}\right)$ represents the lth-order directional derivative with respect to the noise operators $E_{j_1},\dots,E_{j_l}$, $\lambda_{j_1,\dots,j_l}^l$ denotes the corresponding weighting coefficient, and $\|\cdot\|$ stands for the Frobenius norm. The weighting coefficients should be set according to the relative significance of the directional derivatives, and are tuned during the optimization procedure. The task then becomes a multiobjective optimization problem.

Generally speaking, there exist various optimization algorithms that can be applied to search optimal controls for maximizing $\Phi(u)$. Here, we choose the famous GRAPE algorithm [31], which has been widely applied in many quantum engineering tasks [36–38]. Combined with the Van Loan integral formula for calculating the directional derivatives, the optimization algorithm we use in this work is called Van Loan GRAPE for short. The flowchart of this algorithm is shown in Fig. 1. Meanwhile, we briefly describe its algorithm procedures as follows:

Step 1. Set the weighting coefficients $\lambda_{j_1,\dots,j_l}^l$ of the multiobjective fitness function $\Phi(u)$ with appropriate values, randomly initialize the piecewise-constant control fields $u = (u[m]), m = 1,\dots,M$.

Step 2. Evaluate $\Phi(u)$, if not sufficiently high, iteratively do the following steps:

(1) Calculate the gradients of $\Phi(u)$ with respect to u, namely $\partial\Phi/\partial u[m]$.
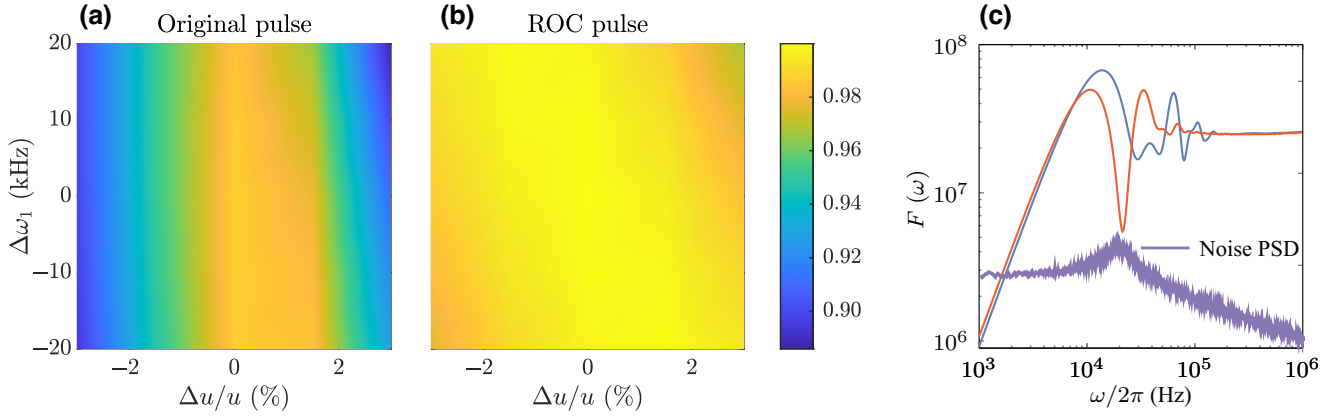
FIG. 2. Performance comparison of the original and the robust MS gate under the coexistence of three types of noises. (a),(b) demonstrate the gate fidelities with respect to the varying Rabi-frequency fluctuation and motional mode frequency fluctuation. (c) PSD of the tested noise, and filter functions of the original and the ROC pulse. The time-dependent qubit-frequency detuning is simulated using the parameters $\omega'/2\pi = 2 \times 10^4$ Hz, $A/2\pi = 2 \times 10^4$ Hz. All simulations are conducted in a 72-dimension space where the number of phonons is considered to be 5 and 2, respectively.

(2) Update the control fields with $u[m] \leftarrow u[m] + p\,\partial\Phi/\partial u[m]$, where p is a suitably chosen step length.

Step 3. Evaluate $\Phi_0(u)$, if not sufficiently high, then modify $\lambda^l_{j_1,...,j_l}$ and go to *Step 2*.

Step 4. Output the optimal control fields u.

In addition, we add the following two constraints during the optimization, so as to meet the requirements of practical applications: (1) bounded control amplitude by setting $|u[m]| \leq \Omega_{\max}, m = 1, 2, \ldots, M$; (2) smooth control amplitude by requiring the amplitude difference between two adjacent segments to be small.

III. ROBUST MØLMER-SØRENSEN GATE ON TRAPPED IONS

Trapped ions are considered to be one of the most promising qubit platforms for quantum computation [39]. This is due to their long coherence times compared to the operation time, as well as their ability to achieve high-quality initialization and readout [40,41]. High-fidelity two-qubit entangling gates are essential for universal quantum computation, thus have been extensively studied in trapped ions [42–45]. However, various noises, such as Rabi errors and motional heating, can substantially reduce the gate fidelities. To tackle this issue, there have been a number of works focused on developing robust two-qubit gates, but mostly are designed for one to two types of noises and are not easy to analytically derive. [46–50]. Here, we demonstrate that using the robust quantum optimal control method, high-fidelity two-qubit gates on ion traps can be realized under frequently encountered noises.

Consider two ions interacting with a laser field of frequency ω_l. The system's Hamiltonian is described by the equation $H_S = \omega_0 \sum_{k=1}^2 \sigma_z^k/2 + \sum_{j=1}^2 \nu_j \hat{a}_j^\dagger \hat{a}_j$, where $\sigma_{x,y,z}^k$

are the Pauli matrixes for the kth qubit, ν_j is the eigenfrequency of the jth collective motional modes and $\hat{a}_j^\dagger, \hat{a}_j$ are the corresponding ladder operators. For convenience, we transform to the ions' resonant rotating frame defined by $e^{-it\omega_0 \sum_{k=1}^2 \sigma_z^k/2}$, thus the system Hamiltonian becomes

$$H_S = \sum_{j=1}^2 \nu_j \hat{a}_j^\dagger \hat{a}_j. \tag{14}$$

With rotating-wave approximation, the control Hamiltonian can then be expressed as [51]

$$H_C = \frac{1}{2} \sum_{k=1}^2 u_k(t)\sigma_+^k e^{i[\sum_{j=1}^2 \eta_j(\hat{a}_j + \hat{a}_j^\dagger) - \omega t]} + \text{h.c.}, \tag{15}$$

where $\sigma_+^k = \sigma_x^k + i\sigma_y^k$, $\omega = \omega_l - \omega_0$, $u_k(t)$ represents Rabi frequency, and η_j is the Lamb-Dicke parameter. Routinely, we restrict to Lamb-Dicke regime [39], thus the above equation can be approximated as

$$H_C = \sum_{k=1}^2 u_k(t)\cos(\omega t)\left[\sigma_x^k + \sum_{j=1}^2 \eta_j(\hat{a}_j + \hat{a}_j^\dagger)\sigma_y^k\right].$$

Suppose that our target is to implement an entangling gate $U_{\text{tar}} = \exp\left(i\pi\sigma_y^1\sigma_y^2/4\right)$ using the MS scheme [45, 52]. The original MS gate requires a bichromatic laser field close to one of the motional sidebands, e.g., $\omega_l \approx \omega_0 \pm \nu_1$, and we define $\omega_l - \omega_0 \pm \nu_1 \equiv \pm\delta$. Moreover, the Rabi frequency is assumed to be constant and not too strong, i.e., $u_1(t) = u_2(t) \equiv \Omega$, $\eta\Omega \ll \delta$ and $\eta_1 = \eta_2 = \eta$. As such, the system undergoes an adiabatic process, during which the intermediate states will not be populated.

By perturbation theory, we obtain an effective Hamiltonian $H_{\text{eff}} = \eta^2\Omega^2/(2\delta)\sigma_y^1\sigma_y^2$. Clearly, if we drive the system for a total time $T_{\text{MS}} = \pi\delta/(2\eta^2\Omega^2)$, we can achieve the target MS gate. The drawback of adiabatic driving is that the gate time is relatively long. A direct way to reduce the gate time is just by decreasing δ and increasing Ω, and meanwhile making sure that the motional modes are not excited at the end of the evolution. This approach enables us to achieve a relatively fast MS gate, as documented in Ref. [53]; we mark the control waveform obtained in this way as "original pulse." Nevertheless, this original MS gate easily suffers from various noises. We thus use the ROC method introduced above to achieve a robust MS gate through modulating $u_k(t)$.

A. Three types of realistic noises under consideration

In our investigation, we examine the coexistence of two types of static noises and one time-dependent noise in trapped ions. The first one is the Rabi-frequency fluctuation [49,54], which originates from fluctuations in the laser power or phase, and imperfections in the optics or electronics. In general, the bichromatic field consisting of a pair of copropagating lasers can be subject to distinct noise. For simplicity, we assume the presence of identical noise in both lasers exciting the red and blue sidebands, which can be modeled by $H_{V_1}(t) = \Delta u H_C(t)$. It is worth noting that the Van Loan GRAPE algorithm remains adaptable, allowing for situations where Rabi-frequency fluctuations of red and blue sideband are different. The second one is the frequency fluctuation of the motional modes [55–57], which is caused by fluctuations in the trapping potential, couplings to the external environments and variations in the ion's position. It can be descried by $H_{V_2}(t) = \Delta\omega_1\hat{a}_1^\dagger\hat{a}_1$. The third one is the qubit-frequency detuning [46,48], which may come from drift of the trapped fields and fluctuations of magnetic field in the environment. This noise can be modeled by $H_{V_3}(t) = \epsilon_{\omega_0}(t)E(t)$ with $E(t) = \sum_{k=1}^{2}\sigma_z^k/2$. As described above, we assume that $\epsilon_{\omega_0}(t)$ is a stationary Gaussian process with zero mean, and its properties can be characterized by the autocorrelation function $\langle\epsilon_{\omega_0}(t)\epsilon_{\omega_0}(t+\tau)\rangle$. Overall, the perturbed Hamiltonian is $H_V(t) = H_{V_1}(t) + H_{V_2}(t) + H_{V_3}(t)$. To search smooth pulses that demonstrate robustness against these noises, we parameterize the control fields and utilize Gaussian smoothing method to ensure the pulses are sufficiently smooth. The method described in Sec. II is then applied to optimize the controls $u(t)$ for realizing the robust MS gate. The details about fitness function and gradients are given in the Appendix.

B. Simulation results

The searched ROC pulse, which exhibits a smooth envelope suitable for experimental implementation, is
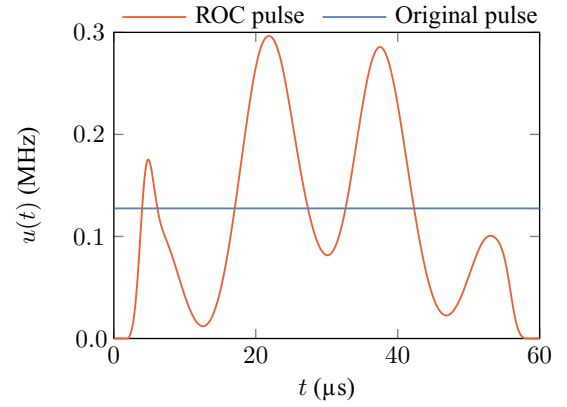

FIG. 3. Waveforms of the original and the robust pulse for realizing the MS gate. The original pulse is simulated using parameters $\eta = 0.1$, $\omega = 0.983\nu_1$, $\Omega = 0.1275$ MHz, $\nu_1 = 2$ MHz and $\nu_2 = 2\sqrt{2}$ MHz. The ROC pulse is simulated using parameters $\eta = 0.1$, $\omega = 0.983\nu_1$, $T = 60$ μs, $M = 600$, $\nu_1 = 2$ MHz, and $\nu_2 = 2\sqrt{3}$ MHz.

illustrated in Fig. 3. We first compare the robustness of the original and the robust pulse under varying Rabi-frequency fluctuations (-3% to 3%) and motional mode frequency fluctuations (-20 to 20 kHz), as shown in Figs. 2(a) and 2(b), respectively. It is clear that the robust region for the ROC pulse is much larger than that for the original pulse. This indicates that our ROC pulse can simultaneously resist two types of static noises for improving the gate performance. Moreover, even when $\Delta u/u = 0$ and $\Delta\omega_1 = 0$ Hz, the gate fidelity of the robust MS gate is much higher than that of the original MS gate. This is due to the fact that the modulation of the ROC pulse enhances the control abilities compared to the rectangular original pulse.

Subsequently, we assess the robustness of the ROC pulse to the considered time-dependent noise. For convenience, we move to frequency domain using the filter-function formalism [33,34]. Specifically, the fitness function in Eq. (4) can be expressed in the following form:

$$\Phi_{\text{noise}}(u) = 1 - \frac{1}{2\pi}\int_{-\infty}^{\infty}\frac{d\omega}{\omega^2}S(\omega)F(\omega), \quad (16)$$

where $S(\omega)$ is the so-called power spectral density (PSD), which is the Fourier transformation of the autocorrelation function $\langle\epsilon_{\omega_0}(t)\epsilon_{\omega_0}(t+\tau)\rangle$ and defined by $S(\omega) = \int_{-\infty}^{\infty}d\tau e^{-i\omega\tau}\langle\epsilon_{\omega_0}(t)\epsilon_{\omega_0}(t+\tau)\rangle$. The control filter function $F(\omega)$ can be calculated by

$$F(\omega) = \sum_k\left|-i\omega\int_0^T dt\,\text{Tr}\left\{\mathcal{S}^\dagger\widetilde{E}_{\text{full}}(t)\mathcal{S}P_k/2^2\right\}e^{i\omega t}\right|^2,$$

where $\{P_k\}_{k=0}^{4^2-1} = \{\mathbb{1},\sigma_x,\sigma_y,\sigma_z\}^{\otimes 2}$ are Pauli matrices, $\widetilde{E}_{\text{full}}(t) = U^\dagger(t)(E(t)\otimes\mathbb{1}_\nu)U(t)$ represents the full-space

TABLE I. Gate fidelities of the original and the robust MS gate when the tested three types of noises coexist.

$\Delta u/u$ (%)	0.5	1.0	1.5	2.0	2.5
$\Delta\omega_1$ (kHz)	0.5	1.0	1.5	2.0	2.5
$\sqrt{\langle \varepsilon_{\omega_0}^2(t)\rangle}$ (kHz)	2	4	6	8	10
$\Phi_{\text{noise}}^{\text{original}}$	0.9830	0.9770	0.9697	0.9612	0.9518
$\Phi_{\text{noise}}^{\text{ROC}}$	0.9999	0.9999	0.9997	0.9995	0.9993

noise operator (toggling frame) with $\mathbb{1}_\nu$ being the identity operators of the motional-mode subspaces. The operator $\mathcal{S}$ projects the full-space time-evolution operator into the qubit subspaces. Thus, it provides an effective way to evaluate the quality of a designed control by analyzing the degree of overlap between $S(\omega)$ and $F(\omega)$. In practice, truncation is necessary to calculate the ladder operators $\hat{a}$ and $\hat{a}^\dagger$. We truncate them by considering the phonon number up to five for first motional mode and two for second motional mode in our simulations. For simplicity, we consider Lorentzian-type PSD, i.e., $S(\omega) \propto 1/(A^2 + (\omega - \omega')^2)$ [55,56], as shown in Fig. 2(c) (marked as "Noise PSD"). The filter functions of the original pulse and the ROC pulse are depicted in Fig. 2(c). It is evident that the filter function of the ROC pulse has a sharp dip at the characteristic frequency of the noise spectrum, indicating a better performance in resisting this time-dependent noise.

Moreover, we present the gate fidelities of the MS gate under the influence of all three types of noises in Table I. It is evident that the gate fidelities using the original pulse experience a significant decrease as the noise strength increases. However, with our ROC pulse, the gate fidelities consistently remain above 0.999 in all tested scenarios. This finding highlights the ability of our ROC pulse to effectively resist all three types of noises, thereby enhancing gate performance.

IV. ROBUST CONTROLLED-*Z* GATE FOR SUPERCONDUCTING CIRCUITS

Superconducting circuits are promising for quantum computation due to their ease of fabrication using standard microfabrication techniques, scalability, and ability to achieve long coherence times [58–61]. Two-qubit entangling gates play a crucial role as fundamental components in universal quantum computation and have received significant attention regarding their robustness against various noise sources, including charge noise, magnetic flux noise, and residual couplings [62–64]. Nevertheless, the majority of the existing methods either focus on addressing specific types of noises or encounter challenges when attempting to resist multiple sources of noises simultaneously. Here, we demonstrate that, when several commonly encountered

noises coexist, high-fidelity controlled-*Z* (CZ) gates can be achieved with robust quantum optimal control.

Consider a system of two capacitively coupled transmon superconducting qubits, whose Hamiltonian is of the form [61]

$$H_S = \sum_{i=1}^{2}\left[\omega_i\hat{a}_i^\dagger\hat{a}_i + \frac{\alpha_i}{2}\hat{a}_i^\dagger\hat{a}_i^\dagger\hat{a}_i\hat{a}_i\right] - J(\hat{a}_1 - \hat{a}_1^\dagger)(\hat{a}_2 - \hat{a}_2^\dagger),$$

where ω_i and α_i are the qubit frequency and the anharmonicity of the *i*th qubit, respectively, and J is the coupling strength. Usually, two-qubit entangled gates can be realized through tuning qubit frequencies [64–66] or applying microwave pulses [67,68]. Here, we aim to realize a two-qubit CZ gate $U_{\text{tar}} = |00\rangle\langle00| + |01\rangle\langle01| + |10\rangle\langle10| - |11\rangle\langle11|$ by adjusting the frequency of the first qubit, thus the control Hamiltonian can be described by

$$H_C(t) = u(t)\hat{a}_1^\dagger\hat{a}_1. \tag{17}$$

Conventionally, the CZ gate can be achieved using a trapezoid-shaped pulse in combination with auxiliary single-qubit local rotations, i.e., [69]

$$u(t) = \frac{u_{\text{on}}}{2}\left[\text{erf}\left(\frac{t - t'}{\sigma}\right) - \text{erf}\left(\frac{t + t' - T}{\sigma}\right)\right], \tag{18}$$

where $u_{\text{on}} = \omega_2 - \omega_1 - \alpha_2$, erf represents the error function $\text{erf}(x) = 2/\sqrt{\pi}\int_0^x e^{-t^2}dt$, and the pulse-switching time is determined by σ and t'. This pulse utilizes the avoided crossing between the energy levels $|11\rangle$ and $|02\rangle$ to realize the CZ gate. However, this original pulse may be sensitive to certain noises.

A. Three types of realistic noises under consideration

In our investigation, we assume the presence of two types of static noises and one time-dependent noise. The first noise of consideration is the coupling-strength fluctuation [70,71], which is caused by environmental noises or qubit-frequency drift. This type of noise can be described by $H_{V_1}(t) = \Delta J(\hat{a}_1 - \hat{a}_1^\dagger)(\hat{a}_2 - \hat{a}_2^\dagger)$. The second one is the anharmonicity fluctuation [70], which arises from defects occurring during the fabrication process. It can be modeled by $H_{V_2}(t) = \Delta\alpha_1(\hat{a}_1^\dagger\hat{a}_1^\dagger\hat{a}_1\hat{a}_1)/2$. The third one is the qubit-frequency fluctuation [72]. It originates from ubiquitous charge or flux noise and can be modeled by $H_{V_3}(t) = \epsilon_{\omega_1}(t)E(t)$ with $E(t) = \hat{a}_1^\dagger\hat{a}_1$, where $\epsilon_{\omega_1}(t)$ is a stationary Gaussian process with zero mean. Therefore, the perturbed Hamiltonian can be summarized as $H_V(t) = H_{V_1}(t) + H_{V_2}(t) + H_{V_3}(t)$. We then utilize the method described in Sec. II to search for ROC pulses that can generate robust CZ gates. In addition, we also employ the previously introduced Gaussian smoothing technique. More details about fitness function and gradients can be found in the Appendix.
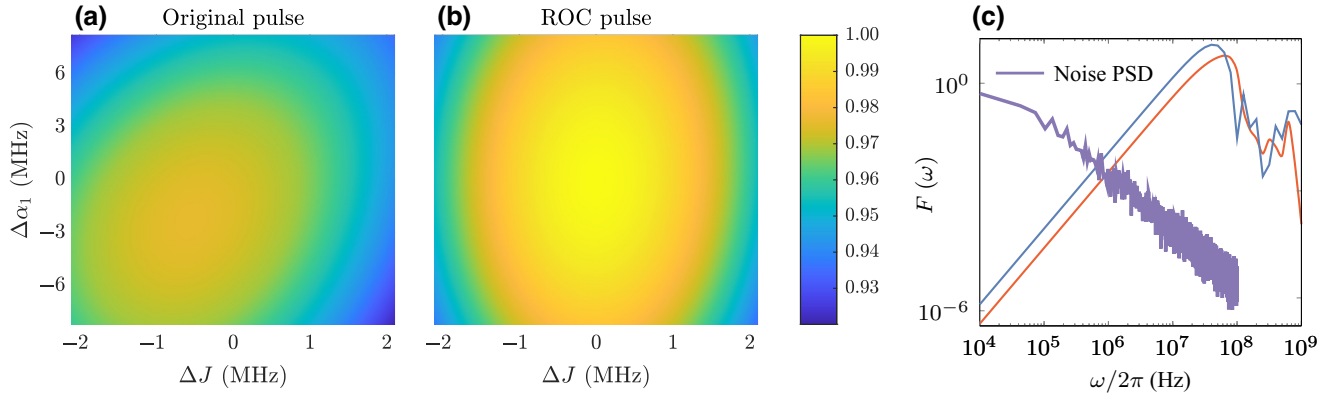
FIG. 4. Performance comparison of the original and the robust CZ gate under the coexistence of three types of noises. (a),(b) demonstrate the gate fidelities regrading the varying coupling-strength fluctuation and anharmonicity fluctuation. (c) PSD of the imported noise, and filter functions of the original and the ROC pulse. The time-dependent qubit-frequency fluctuation is simulated using parameters $\omega_l/2\pi = 1 \times 10^4$ Hz and $\omega_h/2\pi = 1 \times 10^8$ Hz.

B. Simulation results

The obtained ROC pulse exhibits a smooth profile, and thus is suitable for experimental implementations; see Fig. 5. Firstly, we compare the robustness of the original and the ROC pulse under the varying coupling-strength fluctuation and anharmonicity fluctuation, as shown in Figs. 4(a) and 4(b), respectively. We find that the robust region of the ROC pulse is much larger than that of the original pulse, which reveals the effectiveness of our method in simultaneously mitigating the two types of static noises. Similarly, we use the fitness function Eq. (16) to evaluate the control performance under the time-dependent noise. The corresponding control filter function can be
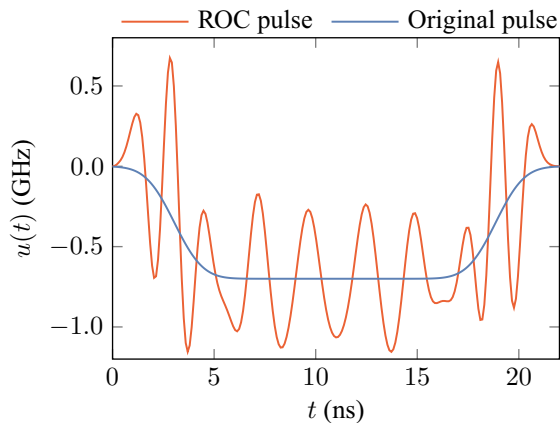
calculated by

$$F(\omega) = \sum_k \left| -i\omega \int_0^T dt \, \mathrm{Tr} \left\{ \mathcal{S}^\dagger \widetilde{E}_{\mathrm{full}}(t) \mathcal{S} P_k / 2^2 \right\} e^{i\omega t} \right|^2,$$

where $\widetilde{E}_{\mathrm{full}}(t) = U^\dagger(t)(E(t) \otimes \mathbb{1}_{\omega_2})U(t)$ is the full-space noise operator (toggling frame) with $\mathbb{1}_{\omega_2}$ being the identity operator of the second-qubit subspace, and $\mathcal{S}$ projects the full-space time-evolution operator into the two-level qubit subspaces. In our simulations, we truncate the ladder operators a and $a^\dagger$ by considering the excited number up to three. The noise spectrum is chosen as $1/f$ type [61], i.e., $S(\omega) \propto 1/\omega \, (\omega_l < \omega < \omega_h)$, where ω_l and ω_h are the low-frequency and the high-frequency cutoffs, respectively. Figure 4(c) presents the results of the original and the robust pulse under the considered time-dependent noise. It can be seen that the ROC pulse has a lower filter function value than the original pulse across the entire frequency domain, indicating a better noise-filtering ability. Furthermore, we present the results when all three types of noises coexist in Table II. It can be seen that the gate fidelities obtained with the original pulse are below 0.975 in all tested cases. In contrast, the gate fidelities achieved with the ROC pulse are all above 0.998. These findings indicate that our ROC pulse possesses the capability to effectively mitigate the impact of all the three types of noises, thus

FIG. 5. Waveforms of the original and the ROC pulse for realizing the CZ gate. The parameters for the original pulse are $u_{\mathrm{on}} = -700$ MHz, $t' = 62.5$ ns, $\sigma = 11.1$ ns. Our ROC pulse is discovered with the parameters $\omega_1 = 7.5$ GHz, $\omega_2 = 6.5$ GHz, $\alpha_1 = -300$ MHz, $\alpha_2 = -300$ MHz, $J = 25$ MHz, $T = 22$ ns, and $M = 220$.

TABLE II. Gate fidelities of the original and the robust CZ gate when the tested three types of noises coexist.

ΔJ (kHz)	10	20	30	40	50
$\Delta\alpha_1$ (MHz)	0.1	0.2	0.3	0.4	0.5
$\sqrt{\langle \varepsilon_{\omega_1}^2(t) \rangle}$ (MHz)	1	2	3	4	5
$\Phi_{\mathrm{noise}}^{\mathrm{original}}$	0.9734	0.9711	0.9685	0.9658	0.9628
$\Phi_{\mathrm{noise}}^{\mathrm{ROC}}$	0.9999	0.9997	0.9994	0.9989	0.9982

leading to considerable enhancement in the overall gate performance.

V. DISCUSSIONS AND OUTLOOK

Achieving high-quality control is critical for quantum computation, but the presence of various inevitable noises poses a significant challenge. Our work demonstrates that robust optimal control offers an effective approach to devise robust quantum gates in scenarios where multiple noises coexist, including static and time dependent. Hence it is our hope that the method can find its experimental applications, and not just limited to the examples of ion traps and superconducting circuits here. Also, the method can be easily applied to other quantum control tasks, such as robust quantum sensing [73] and robust dynamical decoupling [74]. One problem is to extend the method to large-sized systems. As the system size grows, the computational resources required for simulating the system's dynamical evolution will become enormous. Therefore, for future work, we can integrate efficient optimization methods to further enhance our ability to search for robust pulses [75], which could be useful for NISQ applications. Additionally, it may be necessary to explore the effects of pulse shaping on nearby qubits from the considered system qubits [76]. This exploration could reveal potential gate crosstalk that might degrade the performance of the identified robust pulse in realistic applications.

ACKNOWLEDGMENTS

APPENDIX

1. Derivation of Eq. (16) in the main text: filter-function formalism for multiqubit system

For convenience, we consider one time-dependent noise, which is described by $H_V(t) = \epsilon(t)E(t)$. Working in the toggling frame and applying Eq. (7), the gate fidelity in Eq. (4) then becomes

$$\Phi_{\text{noise}}(u) \approx 1 - \frac{1}{d}\int_0^T dt_1 \int_0^T dt_2 \langle \epsilon(t_1)\epsilon(t_2)\rangle \text{Tr}[\tilde{E}(t_1)\tilde{E}(t_2)]. \tag{A1}$$

Noting that $\text{Tr}[\tilde{E}(t)] = \text{Tr}[U^\dagger(t)EU(t)] = \text{Tr}[E] = 0$ and $\tilde{E}(t) = \sum_{k=1}^{d^2} X_k(t)P_k$, where $X_k(t) = \text{Tr}[\tilde{E}(t)P_k]/d$ and $\{P_k\}_{k=0}^{d^2-1} = \{\mathbb{1}_d, \sigma_x, \sigma_y, \sigma_z\}^{\otimes n}$ are Pauli matrices, the above equation can be simplified to

$$\Phi_{\text{noise}}(u) = 1 - \frac{1}{d}\int_0^T dt_1 \int_0^T dt_2 \langle \epsilon(t_1)\epsilon(t_2)\rangle \text{Tr}[\tilde{E}(t_1)\tilde{E}(t_2)]$$

$$= \int_0^T dt_1 \int_0^T dt_2 \int_{-\infty}^\infty d\omega \frac{S(\omega)}{2\pi}e^{i\omega(t_1-t_2)}\sum_{k=0}^{d^2-1} X_k(t_1)X_k(t_2)$$

$$= \frac{1}{2\pi}\sum_{k=0}^{d^2-1}\int_{-\infty}^\infty \frac{d\omega}{\omega^2}S(\omega)R_k(\omega)R_k^*(\omega)$$

$$= \frac{1}{2\pi}\int_{-\infty}^\infty \frac{d\omega}{\omega^2}S(\omega)F(\omega), \tag{A2}$$

where $R_k(\omega) = -i\omega\int_0^T dt\text{Tr}[\tilde{E}(t)P_k/d]e^{i\omega t}$ and $F(\omega) = \sum_{k=1}^{d^2}|R_k(\omega)|^2$. The equation for incorporating multiple noise sources can be derived in a similar manner.

2. Fitness function and gradients of the MS gate function

The fitness function of the MS gate can be explicitly expressed as

$$\Phi(u) = -\lambda_1^{(1)}\left\|\mathcal{D}_U^{(1)}(H_C)\right\|^2 - \lambda_2^{(1)}\left\|\mathcal{D}_U^{(1)}\left(\hat{a}_1^\dagger\hat{a}_1\right)\right\|^2$$

$$- \lambda_3^{(2)}\sum_i a_i\left\|\mathcal{D}_U^{(2)}(e^{b_i}E, e^{-b_i}E)\right\|^2 + \Phi_0(u) + \cdots,$$

where $E = (\sigma_z^1 + \sigma_z^2)/2$. The first and second term denote the first-order effects of the two time-independent noises, the third term represents the effect of the time-dependent noise, and the last one indicates the noise-free gate fidelity. The two block matrices shown in Eqs. (9) and (12) can be explicitly written as

$$B(t) = \begin{pmatrix} H(t) & H_C(t) & 0 \\ 0 & H(t) & a_1^\dagger a_1 \\ 0 & 0 & H(t) \end{pmatrix} \tag{A3}$$

and

$$C_{ji}(t) = \begin{pmatrix} H(t) & \frac{e^{b_{ji}t}}{2}[\sigma_z^1 + \sigma_z^2] & 0 \\ 0 & H(t) & \frac{e^{-b_{ji}t}}{2}[\sigma_z^1 + \sigma_z^2] \\ 0 & 0 & H(t) \end{pmatrix}, \tag{A4}$$

Let the evolution be divided into M slices of equal length $\Delta t = T/M$. Assuming that Δt is small, we can consider the control Hamiltonian, the block matrix Eqs. (A3)

and (A4) to be constant within each slice. Denote the control Hamiltonian and two block matrices at the mth slice as $H_C[m]$, $B[m]$ and $C_{ji}[m]$, respectively. Let $U_m = \exp\{-i\Delta t(H_S + H_C[m])\}$, $V_m = \exp(-i\Delta t B[m])$, $V_{ji_m} = \exp(-i\Delta t C_{ji}[m])$ the total time-evolution operator is then given by $U(T) = U_M \cdots U_1$, $V(T) = V_M \cdots V_1$, $V_{ji}(T) = V_{ji}^{[M]} \cdots V_{ji}^{[1]}$. The Van Loan GRAPE algorithm requires the gradient g of the function $\Phi(u)$ with respect to the control parameters. This gradient can be evaluated according to

$$
\begin{aligned}
g[m] = &-\lambda_1^{(1)} \frac{\partial \left\| \mathcal{D}_U^{(1)}(H_C) \right\|^2}{\partial u[m]} - \lambda_2^{(1)} \frac{\partial \left\| \mathcal{D}_U^{(1)}\left(\hat{a}_1^\dagger \hat{a}_1\right) \right\|^2}{\partial u[m]} - \lambda_3^{(2)} \sum_i a_i \frac{\partial \left\| \mathcal{D}_U^{(2)}(e^{b_i}E, e^{-b_i}E) \right\|^2}{\partial u[m]} + \frac{\partial \Phi_0}{\partial u[m]} - \cdots \\
\approx &-2\lambda_1^{(1)} \operatorname{Re}\left\{ \operatorname{Tr}\left[\left(V_M \cdots \left(-i\Delta t \frac{\partial B[m]}{\partial u[m]}\right) \cdots V_1 \right)\{1,2\} V^\dagger(T)\{1,2\} \right] \operatorname{Tr}^*[V(T)\{1,2\} V^\dagger(T)\{1,2\}] \right\} \\
&-2\lambda_2^{(1)} \operatorname{Re}\left\{ \operatorname{Tr}\left[\left(V_M \cdots \left(-i\Delta t \frac{\partial B[m]}{\partial u[m]}\right) \cdots V_1 \right)\{2,3\} V^\dagger(T)\{2,3\} \right] \operatorname{Tr}^*[V(T)\{2,3\} V^\dagger(T)\{2,3\}] \right\} \\
&-2\lambda_3^{(2)} \sum_i a_i \operatorname{Re}\left\{ \operatorname{Tr}\left[\left(V_{ji}^{[M]} \cdots \left(-i\Delta t \frac{\partial C_{ji}[m]}{\partial u[m]}\right) \cdots V_{ji}^{[1]} \right)\{1,3\} V_{ji}^\dagger(T)\{1,3\} \right] \operatorname{Tr}^*[V_{ji}(T)\{1,3\} V_{ji}^\dagger(T)\{1,3\}] \right\} \\
&+2\operatorname{Re}\left(\operatorname{Tr}\left[U_M \cdots \left(-i\Delta t \frac{\partial H_C[m]}{\partial u[m]}\right) \cdots U_1 U_{\text{tar}}^\dagger \right] \operatorname{Tr}^*[U(T) U_{\text{tar}}^\dagger] \right) + \cdots ,
\end{aligned} \tag{A5}
$$

where $A\{i,j\}$ represents the block matrix of row i and column j of matrix A. For example, in the Eq. (10), $V(T)\{1,2\} = \mathcal{D}_U^{(1)}(E_1)(T)$. More specifically,

$$
\frac{\partial B[m]}{\partial u[m]} = \begin{pmatrix} \frac{\partial H_C[m]}{\partial u[m]} & \frac{\partial H_C[m]}{\partial u[m]} & 0 \\ 0 & \frac{\partial H_C[m]}{\partial u[m]} & 0 \\ 0 & 0 & \frac{\partial H_C[m]}{\partial u[m]} \end{pmatrix},
$$

$$
\frac{\partial C_{ji}[m]}{\partial u[m]} = \begin{pmatrix} \frac{\partial H_C[m]}{\partial u[m]} & 0 & 0 \\ 0 & \frac{\partial H_C[m]}{\partial u[m]} & 0 \\ 0 & 0 & \frac{\partial H_C[m]}{\partial u[m]} \end{pmatrix},
$$

$$
\frac{\partial H_C[m]}{\partial u[m]} = \cos(\omega m \Delta t) \sum_{k=1}^2 \left[\sigma_x^k + \sum_{j=1}^2 \eta_j (\hat{a}_j + \hat{a}_j^\dagger) \sigma_y^k \right].
$$

To accelerate the convergence speed, we apply the quasi-Newton second-order method [77,78] in the optimization process. This can be conveniently implemented using the built-in function "fmincon" in MATLAB, selecting the limited-memory Broyden-Fletcher-Goldfarb-Shanno (LBFGS) option.

3. Fitness function and gradients of the CZ gate function

Here, we consider two time-independent noises and one time-dependent noise. Similarly, for the fitness function, the two block matrices shown in Eqs. (9) and (12) transform into

$$
\begin{aligned}
\Phi(u) = \Phi_0(u) &- \lambda_1^{(1)} \left\| \mathcal{D}_U^{(1)}\left(\hat{a}_1^\dagger \hat{a}_1^\dagger \hat{a}_1 \hat{a}_1\right) \right\|^2 \\
&- \lambda_2^{(1)} \left\| \mathcal{D}_U^{(1)}\left((\hat{a}_1 - \hat{a}_1^\dagger)(\hat{a}_2 - \hat{a}_2^\dagger)\right) \right\|^2 \\
&- \lambda_3^{(2)} \sum_i a_i \left\| \mathcal{D}_U^{(2)}(e^{b_i}E, e^{-b_i}E) \right\|^2 - \cdots ,
\end{aligned}
$$

$$
B(t) = \begin{pmatrix} H(t) & \hat{a}_1^\dagger \hat{a}_1^\dagger \hat{a}_1 \hat{a}_1 & 0 \\ 0 & H(t) & (\hat{a}_1 - \hat{a}_1^\dagger)(\hat{a}_2 - \hat{a}_2^\dagger) \\ 0 & 0 & H(t) \end{pmatrix}
$$

and

$$
C_{ji}(t) = \begin{pmatrix} H(t) & e^{b_{ji}t} \hat{a}_1^\dagger \hat{a}_1 & 0 \\ 0 & H(t) & e^{-b_{ji}t} \hat{a}_1^\dagger \hat{a}_1 \\ 0 & 0 & H(t) \end{pmatrix},
$$

respectively, where $E = \hat{a}_1^\dagger \hat{a}_1$. This gradient can be computed using Eq. (A5) and involves substituting the matrices B and C_{ji} according to the provided expressions. The gradients of $B[m]$, $C_{ji}[m]$ and $H_C[m]$ will also be adjusted using

the following formula:

$$\frac{\partial B[m]}{\partial u[m]} = \begin{pmatrix} \frac{\partial H_C[m]}{\partial u[m]} & \frac{\partial H_C[m]}{\partial u[m]} & 0 \\ 0 & \frac{\partial H_C[m]}{\partial u[m]} & 0 \\ 0 & 0 & \frac{\partial H_C[m]}{\partial u[m]} \end{pmatrix},$$

$$\frac{\partial C_{ji}[m]}{\partial u[m]} = \begin{pmatrix} \frac{\partial H_C[m]}{\partial u[m]} & 0 & 0 \\ 0 & \frac{\partial H_C[m]}{\partial u[m]} & 0 \\ 0 & 0 & \frac{\partial H_C[m]}{\partial u[m]} \end{pmatrix},$$

$$\frac{\partial H_C[m]}{\partial u[m]} = \hat{a}_1^\dagger \hat{a}_1.$$

[1] D. Suter and G. A. Álvarez, Colloquium: Protecting quantum information against environmental noise, Rev. Mod. Phys. **88**, 041001 (2016).

[2] C. Brif, R. Chakrabarti, and H. Rabitz, Control of quantum phenomena: Past, present and future, New J. Phys. **12**, 075008 (2010).

[3] C. Ferrie and O. Moussa, Robust and efficient in situ quantum control, Phys. Rev. A **91**, 052306 (2015).

[4] E. Knill, R. Laflamme, and L. Viola, Theory of quantum error correction for general noise, Phys. Rev. Lett. **84**, 2525 (2000).

[5] J. Preskill, Quantum computing in the NISQ era and beyond, Quantum **2**, 79 (2018).

[6] E. Knill, Quantum computing with realistically noisy devices, Nature **434**, 39 (2005).

[7] E. T. Campbell, B. M. Terhal, and C. Vuillot, Roads towards fault-tolerant universal quantum computation, Nature **549**, 172 (2017).

[8] Y. Li and S. C. Benjamin, Efficient variational quantum simulator incorporating active error minimization, Phys. Rev. X **7**, 021050 (2017).

[9] J. Choi, H. Zhou, H. S. Knowles, R. Landig, S. Choi, and M. D. Lukin, Robust dynamic Hamiltonian engineering of many-body spin systems, Phys. Rev. X **10**, 031002 (2020).

[10] H. K. Cummins, G. Llewellyn, and J. A. Jones, Tackling systematic errors in quantum logic gates with composite rotations, Phys. Rev. A **67**, 042308 (2003).

[11] K. R. Brown, A. W. Harrow, and I. L. Chuang, Arbitrarily accurate composite pulse sequences, Phys. Rev. A **70**, 052318 (2004).

[12] M. Bando, T. Ichikawa, Y. Kondo, and M. Nakahara, Concatenated composite pulses compensating simultaneous systematic errors, J. Phys. Soc. Jpn. **82**, 014004 (2013).

[13] L. Viola, E. Knill, and S. Lloyd, Dynamical decoupling of open quantum systems, Phys. Rev. Lett. **82**, 2417 (1999).

[14] L. Viola and E. Knill, Robust dynamical decoupling of quantum systems with bounded controls, Phys. Rev. Lett. **90**, 037901 (2003).

[15] A. M. Souza, G. A. Álvarez, and D. Suter, Robust dynamical decoupling, Phil. Trans. R. Soc. A **370**, 4748 (2012).

[16] D. Daems, A. Ruschhaupt, D. Sugny, and S. Guérin, Robust quantum control by a single-shot shaped pulse, Phys. Rev. Lett. **111**, 050404 (2013).

[17] G. Dridi, K. Liu, and S. Guérin, Optimal robust quantum control by inverse geometric optimization, Phys. Rev. Lett. **125**, 250403 (2020).

[18] D. Dong, M. A. Mabrok, I. R. Petersen, B. Qi, C. Chen, and H. Rabitz, Sampling-based learning control for quantum systems with uncertainties, IEEE Trans. Control Syst. Technol. **23**, 2155 (2015).

[19] C. Chen, D. Dong, R. Long, I. R. Petersen, and H. A. Rabitz, Sampling-based learning control of inhomogeneous quantum ensembles, Phys. Rev. A **89**, 023402 (2014).

[20] T. Figueiredo Roque, A. A. Clerk, and H. Ribeiro, Engineering fast high-fidelity quantum operations with constrained interactions, Npj Quantum Inf. **7**, 1 (2021).

[21] W. D. Oliver, Engineering a revolution, Nat. Phys. **10**, 794 (2014).

[22] F. K. Malinowski, F. Martins, L. Cywiński, M. S. Rudner, P. D. Nissen, S. Fallahi, G. C. Gardner, M. J. Manfra, C. M. Marcus, and F. Kuemmeth, Spectrum of the nuclear environment for GaAs spin qubits, Phys. Rev. Lett. **118**, 177702 (2017).

[23] K. W. Chan, W. Huang, C. H. Yang, J. C. C. Hwang, B. Hensen, T. Tanttu, F. E. Hudson, K. M. Itoh, A. Laucht, A. Morello, and A. S. Dzurak, Assessment of a silicon quantum dot spin qubit environment via noise spectroscopy, Phys. Rev. Appl. **10**, 044017 (2018).

[24] Y. Sung, F. Beaudoin, L. M. Norris, F. Yan, D. K. Kim, J. Y. Qiu, U. von Lüpke, J. L. Yoder, T. P. Orlando, S. Gustavsson, L. Viola, and W. D. Oliver, Non-Gaussian noise spectroscopy with a superconducting qubit sensor, Nat. Commun. **10**, 3175 (2019).

[25] M. Zhang, Y. Xie, J. Zhang, W. Wang, C. Wu, T. Chen, W. Wu, and P. Chen, Estimation of the laser frequency noise spectrum by continuous dynamical decoupling, Phys. Rev. Applied **15**, 014033 (2021).

[26] J. M. Chow, J. M. Gambetta, L. Tornberg, J. Koch, L. S. Bishop, A. A. Houck, B. R. Johnson, L. Frunzio, S. M. Girvin, and R. J. Schoelkopf, Randomized benchmarking and process tomography for gate errors in a solid-state qubit, Phys. Rev. Lett. **102**, 090502 (2009).

[27] E. Knill, D. Leibfried, R. Reichle, J. Britton, R. B. Blakestad, J. D. Jost, C. Langer, R. Ozeri, S. Seidelin, and D. J. Wineland, Randomized benchmarking of quantum gates, Phys. Rev. A **77**, 012307 (2008).

[28] U. von Lüpke, F. Beaudoin, L. M. Norris, Y. Sung, R. Winik, J. Y. Qiu, M. Kjaergaard, D. Kim, J. Yoder, S. Gustavsson, L. Viola, and W. D. Oliver, Two-qubit spectroscopy of spatiotemporally correlated quantum noise in superconducting qubits, PRX Quantum **1**, 010305 (2020).

[29] H. Haas, D. Puzzuoli, F. Zhang, and D. G. Cory, Engineering effective Hamiltonians, New J. Phys. **21**, 103011 (2019).

[30] C. Van Loan, Computing integrals involving the matrix exponential, IEEE Trans. Automat. Contr. **23**, 395 (1978).

[31] N. Khaneja, T. Reiss, C. Kehlet, T. Schulte-Herbrüggen, and S. J. Glaser, Optimal control of coupled spin dynamics: design of NMR pulse sequences by gradient ascent algorithms, J. Magn. Reson. **172**, 296 (2005).

[32] F. J. Dyson, The radiation theories of Tomonaga, Schwinger, and Feynman, Phys. Rev. **75**, 486 (1949).

[33] M. Biercuk, A. Doherty, and H. Uys, Dynamical decoupling sequence construction as a filter-design problem, J. Phys. B: At. Mol. Opt. Phys. **44,** 154002 (2011).

[34] T. J. Green, J. Sastrawan, H. Uys, and M. J. Biercuk, Arbitrary quantum control of qubits in the presence of universal noise, New J. Phys. **15,** 095004 (2013).

[35] Z.-H. Wang, G. de Lange, D. Ristè, R. Hanson, and V. V. Dobrovitski, Comparison of dynamical decoupling protocols for a nitrogen-vacancy center in diamond, Phys. Rev. B **85,** 155204 (2012).

[36] G. Waldherr, Y. Wang, S. Zaiser, M. Jamali, T. Schulte-Herbrüggen, H. Abe, T. Ohshima, J. Isoya, J. Du, P. Neumann, and J. Wrachtrup, Quantum error correction in a solid-state hybrid spin register, Nature **506,** 204 (2014).

[37] X. Rong, J. Geng, F. Shi, Y. Liu, K. Xu, W. Ma, F. Kong, Z. Jiang, Y. Wu, and J. Du, Experimental fault-tolerant universal quantum gates with solid-state spins under ambient conditions, Nat. Commun. **6,** 8748 (2015).

[38] J. Li, X. Yang, X. Peng, and C.-P. Sun, Hybrid quantum-classical approach to quantum optimal control, Phys. Rev. Lett. **118,** 150503 (2017).

[39] H. Häffner, C. Roos, and R. Blatt, Quantum computing with trapped ions, Phys. Rep. **469,** 155 (2008).

[40] Y. Wang, M. Um, J. Zhang, S. An, M. Lyu, J.-N. Zhang, L.-M. Duan, D. Yum, and K. Kim, Single-qubit quantum memory exceeding ten-minute coherence time, Nat. Photonics **11,** 646 (2017).

[41] T. P. Harty, D. T. C. Allcock, C. J. Ballance, L. Guidoni, H. A. Janacek, N. M. Linke, D. N. Stacey, and D. M. Lucas, High-fidelity preparation, gates, memory, and readout of a trapped-ion quantum bit, Phys. Rev. Lett. **113,** 220501 (2014).

[42] J. I. Cirac and P. Zoller, Quantum computations with cold trapped ions, Phys. Rev. Lett. **74,** 4091 (1995).

[43] F. Schmidt-Kaler, H. Häffner, M. Riebe, S. Gulde, G. P. Lancaster, T. Deuschle, C. Becher, C. F. Roos, J. Eschner, and R. Blatt, Realization of the Cirac–Zoller controlled-not quantum gate, Nature **422,** 408 (2003).

[44] D. Leibfried, B. DeMarco, V. Meyer, D. Lucas, M. Barrett, J. Britton, W. M. Itano, B. Jelenković, C. Langer, T. Rosenband, and D. J. Wineland, Experimental demonstration of a robust, high-fidelity geometric two ion-qubit phase gate, Nature **422,** 412 (2003).

[45] A. Sørensen and K. Mølmer, Quantum computation with ions in thermal motion, Phys. Rev. Lett. **82,** 1971 (1999).

[46] T. Manovitz, A. Rotem, R. Shaniv, I. Cohen, Y. Shapira, N. Akerman, A. Retzker, and R. Ozeri, Fast dynamical decoupling of the Mølmer-Sørensen entangling gate, Phys. Rev. Lett. **119,** 220505 (2017).

[47] P. H. Leung, K. A. Landsman, C. Figgatt, N. M. Linke, C. Monroe, and K. R. Brown, Robust 2-qubit gates in a linear ion crystal using a frequency-modulated driving force, Phys. Rev. Lett. **120,** 020501 (2018).

[48] Y. Shapira, R. Shaniv, T. Manovitz, N. Akerman, and R. Ozeri, Robust entanglement gates for trapped-ion qubits, Phys. Rev. Lett. **121,** 180502 (2018).

[49] T. J. Green and M. J. Biercuk, Phase-modulated decoupling and error suppression in qubit-oscillator systems, Phys. Rev. Lett. **114,** 120502 (2015).

[50] A. E. Webb, S. C. Webster, S. Collingbourne, D. Bretaud, A. M. Lawrence, S. Weidt, F. Mintert, and W. K. Hensinger, Resilient entangling gates for trapped ions, Phys. Rev. Lett. **121,** 180501 (2018).

[51] P. J. Lee, K.-A. Brickman, L. Deslauriers, P. C. Haljan, L.-M. Duan, and C. Monroe, Phase control of trapped ion quantum gates, J. Opt. B: Quantum Semiclass. Opt. **7,** S371 (2005).

[52] K. Mølmer and A. Sørensen, Multiparticle entanglement of hot trapped ions, Phys. Rev. Lett. **82,** 1835 (1999).

[53] A. Sørensen and K. Mølmer, Entanglement and quantum computation with ions in thermal motion, Phys. Rev. A **62,** 022311 (2000).

[54] J. P. Gaebler, T. R. Tan, Y. Lin, Y. Wan, R. Bowler, A. C. Keith, S. Glancy, K. Coakley, E. Knill, D. Leibfried, and D. J. Wineland, High-fidelity universal gate set for $^9Be^+$ ion qubits, Phys. Rev. Lett. **117,** 060505 (2016).

[55] A. R. Milne, C. L. Edmunds, C. Hempel, F. Roy, S. Mavadia, and M. J. Biercuk, Phase-modulated entangling gates robust to static and time-varying errors, Phys. Rev. Appl. **13,** 024022 (2020).

[56] A. R. Milne, C. Hempel, L. Li, C. L. Edmunds, H. J. Slatyer, H. Ball, M. R. Hush, and M. J. Biercuk, Quantum oscillator noise spectroscopy via displaced cat states, Phys. Rev. Lett. **126,** 250506 (2021).

[57] M. Kang, Y. Wang, C. Fang, B. Zhang, O. Khosravani, J. Kim, and K. R. Brown, Designing filter functions of frequency-modulated pulses for high-fidelity two-qubit gates in ion chains, Phys. Rev. Appl. **19,** 014014 (2023).

[58] J. Clarke and F. K. Wilhelm, Superconducting quantum bits, Nature **453,** 1031 (2008).

[59] M. H. Devoret and R. J. Schoelkopf, Superconducting circuits for quantum information: An outlook, Science **339,** 1169 (2013).

[60] M. Kjaergaard, M. E. Schwartz, J. Braumüller, P. Krantz, J. I.-J. Wang, S. Gustavsson, and W. D. Oliver, Superconducting qubits: Current state of play, Annu. Rev. Condens. Matter Phys. **11,** 369 (2020).

[61] P. Krantz, M. Kjaergaard, F. Yan, T. P. Orlando, S. Gustavsson, and W. D. Oliver, A quantum engineer's guide to superconducting qubits, Appl. Phys. Rev. **6,** 021318 (2019).

[62] F. Yan, P. Krantz, Y. Sung, M. Kjaergaard, D. L. Campbell, T. P. Orlando, S. Gustavsson, and W. D. Oliver, Tunable coupling scheme for implementing high-fidelity two-qubit gates, Phys. Rev. Appl. **10,** 054062 (2018).

[63] Y. Xu, J. Chu, J. Yuan, J. Qiu, Y. Zhou, L. Zhang, X. Tan, Y. Yu, S. Liu, J. Li, F. Yan, and D. Yu, High-fidelity, high-scalability two-qubit gate scheme for superconducting qubits, Phys. Rev. Lett. **125,** 240503 (2020).

[64] M. A. Rol, F. Battistel, F. K. Malinowski, C. C. Bultink, B. M. Tarasinski, R. Vollmer, N. Haider, N. Muthusubramanian, A. Bruno, B. M. Terhal, and L. DiCarlo, Fast, high-fidelity conditional-phase gate exploiting leakage interference in weakly anharmonic superconducting qubits, Phys. Rev. Lett. **123,** 120502 (2019).

[65] F. W. Strauch, P. R. Johnson, A. J. Dragt, C. J. Lobb, J. R. Anderson, and F. C. Wellstood, Quantum logic gates for coupled superconducting phase qubits, Phys. Rev. Lett. **91,** 167005 (2003).

[66] L. DiCarlo, J. M. Chow, J. M. Gambetta, L. S. Bishop, B. R. Johnson, D. Schuster, J. Majer, A. Blais, L. Frunzio, S. Girvin, and R. J. Schoelkopf, Demonstration of two-qubit algorithms with a superconducting quantum processor, Nature **460,** 240 (2009).

[67] J. M. Chow, A. D. Córcoles, J. M. Gambetta, C. Rigetti, B. R. Johnson, J. A. Smolin, J. R. Rozen, G. A. Keefe, M. B. Rothwell, M. B. Ketchen, and M. Steffen, Simple all-microwave entangling gate for fixed-frequency superconducting qubits, Phys. Rev. Lett. **107,** 080502 (2011).

[68] G. S. Paraoanu, Microwave-induced coupling of superconducting qubits, Phys. Rev. B **74,** 140504 (2006).

[69] J. Ghosh, A. Galiautdinov, Z. Zhou, A. N. Korotkov, J. M. Martinis, and M. R. Geller, High-fidelity controlled-σ^Z gate for resonator-based superconducting quantum computers, Phys. Rev. A **87,** 022309 (2013).

[70] D. J. Egger and F. K. Wilhelm, Optimized controlled-z gates for two superconducting qubits coupled through a resonator, Supercond. Sci. Technol. **27,** 014001 (2013).

[71] P. Zhao, P. Xu, D. Lan, J. Chu, X. Tan, H. Yu, and Y. Yu, High-contrast zz interaction using superconducting qubits with opposite-sign anharmonicity, Phys. Rev. Lett. **125,** 200503 (2020).

[72] L. Cywiński, R. M. Lutchyn, C. P. Nave, and S. Das Sarma, How to enhance dephasing time in superconducting qubits, Phys. Rev. B **77,** 174509 (2008).

[73] F. Poggiali, P. Cappellaro, and N. Fabbri, Optimal control for one-qubit quantum sensing, Phys. Rev. X **8,** 021059 (2018).

[74] X. Yang, Y. Ge, B. Zhang, and J. Li, Robust dynamical decoupling for the manipulation of a spin network via a single spin, Phys. Rev. Appl. **18,** 054075 (2022).

[75] J. Li, Subsystem-based approach to scalable quantum optimal control, arXiv:1910.02061.

[76] C. Fang, Y. Wang, S. Huang, K. R. Brown, and J. Kim, Crosstalk suppression in individually addressed two-qubit gates in a trapped-ion quantum computer, Phys. Rev. Lett. **129,** 240504 (2022).

[77] R. Eitan, M. Mundt, and D. J. Tannor, Optimal control with accelerated convergence: Combining the Krotov and quasi-Newton methods, Phys. Rev. A **83,** 053426 (2011).

[78] P. De Fouquieres, S. G. Schirmer, S. J. Glaser, and Ilya Kuprov, Second order gradient ascent pulse engineering, J. Magn. Reson. **212,** 412 (2011).